Title: Non-selective cation channel activity of aquaporin AtPIP2;1 regulated by Ca^{2+} and pH

Running title: Aquaporin ion channel

Caitlin S Byrt[1#], Manchun Zhao[1#], Mohamad Kourghi[2], Jayakumar Bose[1], Sam W. Henderson[1], Jiaen Qiu[1], Matthew Gilliham[1], Carolyn Schultz[3], Manuel Schwarz[1], Sunita A Ramesh[1#], Andrea Yool[2#], Steve Tyerman[1#]*

[#] Equal contribution.

[1]Australian Research Council Centre of Excellence in Plant Energy Biology, Waite Research Institute and School of Agriculture, Food and Wine, The University of Adelaide, PMB1, Glen Osmond, SA 5064, Australia.

[2]Discipline of Physiology, School of Medicine, Medical School South, Frome Road, University of Adelaide, SA 5005, Australia.

[3]Waite Research Institute and School of Agriculture, Food and Wine, The University of Adelaide, PMB1, Glen Osmond, SA 5064, Australia.

*Corresponding author: Steve Tyerman

Tel: +61 8 3136663

email: steve.tyerman@adelaide.edu.au

This article has been accepted for publication and undergone full peer review but has not been through the copyediting, typesetting, pagination and proofreading process which may lead to differences between this version and the Version of Record. Please cite this article as doi: 10.1111/pce.12832

ABSTRACT

The aquaporin AtPIP2;1 is an abundant plasma membrane intrinsic protein in *Arabidopsis thaliana* implicated in stomatal closure, but is also highly expressed in plasma membranes of root epidermal cells. When expressed in *Xenopus laevis* oocytes, AtPIP2;1 increased water permeability and induced a non-selective cation conductance mainly associated with Na^+. A mutation in the water pore, G103W, prevented both the ionic conductance and water permeability of PIP2;1. Co-expression of AtPIP2;1 with AtPIP1;2 increased water permeability but abolished the ionic conductance. AtPIP2;2 (93% identical to AtPIP2;1) similarly increased water permeability but not ionic conductance. The ionic conductance was inhibited by the application of extracellular Ca^{2+} and Cd^{2+}, with Ca^{2+} giving a biphasic dose-response with a prominent IC50 of 0.32 mM comparable to a previous report of Ca^{2+}-sensitivity of a non-selective cation channel (NSCC) in Arabidopsis root protoplasts. Low external pH also inhibited ionic conductance (IC50 pH 6.8). *Xenopus* oocytes and *Saccaromyces cerevisiae* expressing AtPIP2;1 accumulated more Na^+ than controls. Establishing whether AtPIP2;1 has dual ion and water permeability *in planta* will be important in understanding the roles of this aquaporin, and if AtPIP2;1 is a candidate for a previously reported NSCC responsible for Ca^{2+} and pH sensitive Na^+ entry into roots.

Keywords: Aquaporin, ion transport, plasma membrane, PIP, water transport, root, non-selective cation channel+

SUMMARY

The paradigm that aquaporins may only allow permeation of neutral solutes has been challenged by examples of some animal aquaporins that can act as ion channels. Here we reveal that AtPIP2;1 is permeable to both water and Na^+ in heterologous systems. The AtPIP2;1 ionic conductance is inhibited by low pH and Ca^{2+} similar to previous observations for non-selective cation channels indicating that AtPIP2;1 is a candidate for facilitating Na^+ flux across the plasma membrane of root cells and other cells that express PIP2;1, such as guard cells.

INTRODUCTION

Plant aquaporins are membrane proteins that transport water and a range of neutral solutes. Some aquaporins transport only water and others transport gases (carbon dioxide, ammonia), metalloids (boron, silicon, arsenic), or reactive oxygen species (hydrogen peroxide) (Uehlein et al., 2003; Loqué et al., 2005; Ma et al., 2006; Takano et al., 2006; Dynowski et al., 2008; Kamiya et al., 2009). A subset of animal aquaporins transport water and ions (Yool and Campbell, 2012), but there is limited evidence of transport of ions by plant aquaporins (Weaver et al., 1994; Rivers et al., 1997; Holm et al., 2005). If a subset of aquaporins co-transport water and ions *in planta* then there may be novel roles for aquaporins in plant nutrient transport and osmotic adjustment.

Root water uptake and stress induced inhibition of root hydraulic conductivity is mediated by plasma membrane intrinsic proteins (PIPs) (Tournaire-Roux et al., 2003). One of the most highly expressed aquaporins in *Arabidopsis* roots is AtPIP2;1 (Alexandersson et al. 2005). AtPIP2;1 is a plasma membrane intrinsic protein that facilitates the transport of water across the plasma membrane. The function of AtPIP2;1 is important for maintaining whole

plant water status, and the water channel activity is inhibited by divalent cations (Verdoucq et al., 2008). For example, when AtPIP2;1 is mislocalized in the endoplasmic reticulum instead of the plasma membrane, a 36-45% reduction in root hydraulic conductivity is observed (Sorieul et al., 2011). In Arabidopsis, root plasma membrane vesicles show water channel activity that is inhibited by Ca^{2+} with an IC_{50} of 75 μM (Gerbeau et al., 2002), and similarly in AtPIP2;1-expressing proteoliposomes water channel activity is inhibited by Ca^{2+}, with an IC_{50} of 42 μM (+/−25 μM) (Verdoucq et al., 2008). A range of divalent cations inhibited the osmotic water permeability of AtPIP2;1 expressing proteoliposomes, particularly Ca^{2+}, Cd^{2+} and Mn^{2+}, and the permeability to water was blocked by H^+, with a half-inhibition at pH 7.15 (Verdoucq et al., 2008). AtPIP2;1 is also important for light-dependent changes in leaf water transport, where hydraulic conductivity in the rosette under darkness is influenced by PIP2;1 phosphorylation at Ser-280 and Ser-283 (Prado et al., 2013).

When Arabidopsis roots are exposed to salt the abundance and phosphorylation status of PIP2;1 changes. NaCl treatment increases the trafficking of AtPIP2 isoforms between the plasma membrane and intracellular compartments, reducing the abundance of PIP2 proteins on the plasma membrane and the hydraulic conductivity of salt-stressed root cells (Boursiac et al., 2005; Sutka et al., 2011). A rapid (half-time, 45 min) decrease (–70%) in root hydraulic conductivity was observed after exposure to 100 mM NaCl (Boursiac et al., 2005). In standard conditions Arabidopsis roots contain poly-phosphoryated, singly phosphorylated, and dephosphorylated forms of AtPIP2;1 in a relative abundance ratio of 1:1:2 (Prak et al., 2008). NaCl acts on AtPIP2;1 with unphosphorylated Ser^{283} to favour intracellular accumulation. NaCl treatment resulted in a 30% decrease in the level of Ser^{283} phosphorylation and an increase in the relative abundance of singly and unphosphorylated forms (Prak et al., 2008). The physiological importance of salt induced cycling of AtPIP2;1 in standard conditions, or

under environmental stresses is not yet clear (Verdoucq et al., 2014). If Na^+ permeated AtPIP2;1 *in planta* then internalization of AtPIP2;1 from the root epidermal plasma membrane in response to salt stress could be a mechanism to avoid Na^+ accumulation.

Given that a non-selective cation channel in the plasma membrane of protoplasts isolated from Arabidopsis roots was inhibited by Ca^{2+} and low pH (Demidchik and Tester, 2002), and that both Ca^{2+} and low pH have been reported to inhibit water channel activity of AtPIP2;1 (Verdoucq et al., 2008; Tournaire-Roux et al., 2003) we investigated if AtPIP2;1 could confer a cation conductance when expressed in heterologous systems and if this was sensitive to Ca^{2+} and external pH. Here we report that in heterologous systems AtPIP2;1 induces a Na^+ conductance that is inhibited by external Ca^{2+} and low external pH.

MATERIALS AND METHODS

Chemicals

All chemicals were supplied by Sigma except where stated otherwise.

Cloning, preparation of constructs and cRNA

Complementary DNA made from RNA extracted from *Arabidopsis thaliana* (Col-0) was used to amplify fragments coding for the plasma membrane intrinsic (PIP) proteins of interest. The primers used for amplification of *AtPIP2;1* (At3g53420), *AtPIP1;2* (At2g45960), *AtPIP1;4* (At4g00430), *AtPIP1;5* (At4g23400), *AtPIP2;2* (At2g37170), *AtPIP2;6* (At2g39010) and generating the G103W *AtPIP2;1* mutant by site-directed mutagenesis are reported in Table S1. Previous research indicated that the AtPIP2;1 G103W mutation blocks the water pore (Shelden et al., 2009). Standard PCR conditions were used (98°C for 30 s, 25 cycles of 98°C for 10 s, 55°C for 30 s, 72°C for 30 s; final extension 72°C for 10 min for AtPIP2;1) with Phusion High-Fidelity DNA Polymerase. The amplified

products were cloned into pENTR TOPO® vector using a pENTR Directional TOPO® Cloning Kit (Invitrogen), transformed into chemically competent Escherichia coli One shot® TOPO10 cells (Invitrogen). AtPIP2;1 cDNA was then recombined by Gateway LR recombination reactions using LR Clonase™ into pGEMHE-DEST (Gateway enabled) following Preuss et al. (2011), and the pYES3-DEST expression vector, transformed into *E. coli* and confirmed by sequencing. pYES3-DEST (Shelden et al., 2009) is a modified version of pYES2 (Invitrogen) converted to a Gateway enabled vector using the Gateway Vector Conversion System (Invitrogen). It has the GAL1 promoter for galactose inducible expression and the URA3 gene for uracil selection. Plasmid DNA was extracted using a Sigma Genelute Plasmid Purification Kit. 1 µg quantities of pGEMHE-DEST plasmid DNA containing the genes of interest were linearized, in preparation for cRNA synthesis, with the restriction enzyme Nhe I or Sph I (New England BioLabs).

A DNA fragment encoding the AtPIP2.1-mCherry fusion protein was PCR amplified from the binary vector PM-RK (Nelson et al., 2007) using Phusion high-fidelity polymerase. The reaction consisted of 5 ng plasmid template, 0.2 units of Phusion polymerase and 500 nM forward (5'-ATGGCAAAGGATGTGGAAG-3') and reverse (5'-TTAAGATCTGTACAGCTCGTCC -3') primers. The PCR fragment was A-tailed with *Taq* polymerase (New England Biolabs), subcloned into pCR8/GW/TOPO (Life Technologies), and recombined into the *Xenopus laevis* expression vector pGEMHE-DEST (Shelden et al., 2009) using LR Clonase II enzyme (Life Technologies). The pGEMHE expression vector harbouring AtPIP2.1-mCherry was linearised with NheI restriction endonuclease, purified by phenol/chloroform extraction and used as a template for *in vitro* Capped RNA (cRNA) synthesis. cRNA was synthesised using the mMESSAGE mMACHINE T7 kit (Ambion) following manufacturer's instructions. The cRNA was purified by phenol/chloroform extraction and was ethanol precipitated and re-suspended in nuclease-free water.

Preparation of *X. laevis* oocytes

Unfertilised oocytes were harvested from *Xenopus laevis* frogs and defoliculated by incubation in collagenase (type 1A, 2 mg/mL) and trypsin inhibitor (1 mg/mL) in 96 mM NaCl, 2 mM KCl, 5 mM $MgCl_2$ and 5 mM HEPES, pH 7.6 for 1 to 1.5 h. The majority of the experiments were conducted in a laboratory in the Plant Research Centre at the Waite Campus, with the exception experiments investigating the influence of varying Ca^{2+} concentrations and solutions with Cd^{2+} on AtPIP2;1 ionic conductance, which were conducted in the Medical School South Building, North Terrace Campus, and the respective differences in protocols are as indicated. At Waite oocytes were stored at 18°C in Ringer's solution: 96 mM NaCl, 2 mM KCl, 5 mM $MgCl_2$, 0.6 mM $CaCl_2$, 5 mM Hepes, 5 % (v/v) horse serum and antibiotics (0.05 mg/mL tetracycline, 100 units/mL penicillin/0.1 mg/mL streptomycin); replaced daily. Oocytes were injected with 46 nL of RNAse-free water using a micro-injector (Nanoinject II, automatic nanolitre injector, Drummond Scientific) with varied concentrations of cRNA (1-25 ng). Water-injected oocytes as controls were included in all experiments. The oocytes were incubated in Ringer's solution as defined above prior to experimentation. In the Medical School South Building oocytes were injected with 50 nL of RNAse-free water containing 0 or 12 ng of AtPIP2;1 cRNA and ooyctes were incubated in 62 mM NaCl, 36 mM KCl, 5 mM $MgCl_2$, 0.6 mM $CaCl_2$, 5 mM HEPES buffer, 5% horse serum, 100 units/mL penicillin, 0.1 mg/mL streptomycin, 0.5 mg/mL tetracycline, pH 7.6 for 1 to 1.5 days prior to experiments. AtPIP2;1 expression was confirmed in a subset of oocytes from each injected batch by swelling tests where AtPIP2;1-cRNA and water injected oocytes were placed in distilled water; AtPIP2;1 expressing oocytes swelled and burst within a few minutes whereas water injected oocytes remained intact for up to 10 min.

Localisation of AtPIP2;1 in *X. laevis* oocytes

Oocytes were injected with 11 ng of AtPIP2;1-mCherry cRNA, or with nuclease-free water, in a total volume of 46 nL. Oocytes were incubated post-injection in Ringer's solution. Oocytes were imaged 2-days post-injection on chambered glass slides using a Zeiss LSM 5 Pascal laser scanning confocal microscope equipped with a Plan-Neofluar 10x/0.3 objective lens. The mCherry fluorophore was excited using a 543 nm HeNe laser. The emission spectrum was collected though a 560 nm long-pass filter. Raw data was processed using Zeiss AIM software (Carl Zeiss).

Water permeability

24 h after injection with cRNA or nuclease-free water oocytes were transferred to 5 mL hypo-osmotic solution, Ringers' solution diluted five fold with sterile water. The osmolality of each solution was determined using a Fiske® 210 Micro-Sample freezing-point osmometer (Advanced Instruments, Inc., USA). Oocytes were viewed with a Nikon SMZ800 light microscope (Nikon, Japan) with the 1.5x objective lens WD45. The changes in volume were captured with a Vicam colour camera (Pacific Communications, Australia) at 2x magnification and recorded with IC Capture 2.0 software (The Imagine Source, US) as AVI format video files. Images were acquired every 3 s for 1.5 min for each oocyte. Image J software (National Institute of Health, USA) was used to calculate the change in total area of the oocytes captured in the AVI video file. Osmotic permeability (P_{os}) was calculated from the increase in volume with time (n = 5-10) using the following equation $P_{os} = V_o(d(V/V_o)/dt) / S*V_w (Osm_{in}-Osm_{out})$, where V_o is the initial oocyte volume (mm^3); $d(V/V_o)/dt$) is the rate of initial relative cell volume change (mm^3/s); S is the initial surface area (mm^3); V_w is the partial molar volume of water 18 cm^3/mol; $Osm_{in}-Osm_{out}$ is the change in osmolality.

Electrophysiology

Two electrode voltage clamp (TEVC) was performed on *Xenopus laevis* oocytes between 24 and 48 h post injection with water, with or without cRNA following Preuss et al. (2011). Borosilicate glass pipettes (Harvard Apparatus, GC150F-10, 1.5 mm O.D. x 0.86 mm I.D.) for voltage and current injecting electrodes were pulled to give between 0.5 to 1 MΩ resistance in ND96 solution (see below) with a filling solution of 3M KCl. A bath clamp system was used to minimize the effect of series resistance in the bath solution. The bath current and voltage sensing electrodes consisted of a silver-silver chloride electrode connected to the bath by 2% agar/3M KCl bridges. The bath solution was continuously perfused during the experiments. Each oocyte was carefully stabbed with the voltage and current electrodes and membrane voltage allowed to stabilise. TEVC experiments were conducted on oocytes with membrane potentials, when in ND96 between –-25 mV and –50 mV and hyperpolarised oocytes with lower membrane potentials were avoided. Voltage clamp experiments were performed with an Oocyte Clamp OC-725C (Warner Instruments) with a Digidata 1440A data aquisition system interface (Axon Instruments) at room temperature (20-22^{o}C). The voltage clamp protocol was set up as follows: –40 mV for 0.5 s, then the membrane potential was decreased in 20 mV steps from 40 mV through to –100 mV or –110 mV, each voltage was held for 2 s, followed by –40 mV for 0.5 s. Recordings were made using a GeneClamp amplifier and Clampex 9.0 software (pClamp 9.0 Molecular Devices, CA, USA). TEVC was initially performed in ND96 solution consisting of 96 mM NaCl, 2 mM KCl, 1 mM $MgCl_2$, 1.8 mM $CaCl_2$, 5 mM HEPES pH 7.5 with TRIS base. Solutions with lower NaCl had otherwise the same composition as ND96 and were made isotonic with ND96 using mannitol. A series of solutions with constant Na^+ concentration of 50 mM and varied Cl^- concentration were made using MES (2-(*N*-morpholino)ethanesulfonic

acid) as a substitute anion. EGTA (ethylene glycol-bis(β-aminoethyl ether)-N,N,N',N'-tetraacetic acid)-buffered divalent free saline (96 mM NaCl, 2 mM KCl, 5 mM HEPES, 10 mM EGTA, pH 7.6) and divalent free salines containing varying EGTA-buffered calcium concentrations were used in experiments with defined and lower Ca^{2+} or Cd^{2+}. The required total concentration of Ca^{2+} needed to achieve the desired free Ca^{2+} concentration in 10 mM EGTA was calculated using http://maxchelator.stanford.edu/CaEGTA-NIST.htm.

Ion-selective microelectrode flux measurements

The water and cRNA injected oocytes were incubated for 48 h in Ringer's solution then the oocytes were transferred to Basal Salt Medium (BSM; 5 mM NaCl, 2 mM KCl, 50 µM $CaCl_2$, 5 mM HEPES) with the osmolality (adjusted with D-mannitol) of 231 mOsmol. Kg^{-1}; the net Na^+ flux was measured non-invasively using ion-selective microelectrodes (the MIFE™ technique; University of Tasmania, Hobart, Australia), as described previously (Newman, 2001). Microelectrode fabrication, conditioning and calibration followed Jayakannan et al. (2011); Bose et al. (2013); Shabala et al. (2013). During measurements, the ion-selective electrodes were positioned using a 3D-micromanipulator (MMT-5, Narishige, Tokyo, Japan), 100 µm from the oocyte surface. A computer-controlled stepper motor moved the electrode between two positions (100 and 200 µm, respectively) from the oocyte surface in 6 s cycles. The CHART software (Newman, 2001) recorded the potential difference between the two positions and converted them into electrochemical potential differences using the calibrated Nernst slope of the electrode. Net ion fluxes were calculated using the MIFEFLUX software for spherical geometry (Newman, 2001).

Yeast growth assay and ion content

The pYES3-DEST-AtPIP2;1 vector and pYES3-DEST empty vector were transformed into *Saccharomyces cerevisiae* strain INVSc2 (Invitrogen) using the LiAc method, and selected on synthetic defined medium without uracil supplemented with 2% (w/v) D-glucose. 20 mL liquid cultures (5.7% (w/v) Yeast Nitrogen Base without amino acids, phosphates or NaCl, MP Biomedicals; 95 $mg.L^{-1}$ L-Histidine-HCL, 1 % (w/v) KH_2PO_4, pH 5.5 with TRIS and either no NaCl, 0.1 M NaCl or 0.5 M NaCl as specified and 2 % (w/v) D-galactose) in 50 mL conical flasks were inoculated with 50 µL of transformed yeast from 1 mL starter cultures with 2% (w/v) D-glucose at an OD_{600} of 0.5. Cultures were grown at 28°C for 24 h at 200 rpm. Cells were extracted by centrifugation (1500 *g*, 3 mins) and washed twice with solution of an equal osmolality (1.1 M sorbitol, 20 mM $MgCl_2$). Cell pellet weight was measured. Pellets were frozen at –20°C for 24 h, then resuspended in 2 mL of MilliQ water and boiled for 30 min to lyse cells. Samples were diluted 1:10 and the Na^+ and K^+ contents of cells grown in liquid culture were measured by flame photometry (model 420 Flame Photometer, Sherwood, Cambridge, United Kingdom).

Statistics

All graphs and statistics were performed in Graphpad Prism 6. All data shown are mean ± SEM. Different letters indicate significance ($P<0.05$) between values as determined by analysis of variance with *post hoc* tests as detailed in the Figure legends or text.

RESULTS

Water permeation through AtPIP2;1 and interaction with AtPIP1;2

Previously AtPIP2;1 has been shown to facilitate water permeability in proteoliposomes (Verdoucq et al., 2008), guard cell protoplasts and *Xenopus laevis* oocytes (Grondin et al., 2015). We confirmed that AtPIP2;1 increased water permeability (P_{os}) in *X. laevis* oocytes and was localised to the plasma membrane (Fig. 1, S1). Various other Arabidopsis PIPs were examined for water permeation; AtPIP2;2, AtPIP2;6, AtPIP1;4, AtPIP1;5 and AtPIP1;2, of which only AtPIP2;2 and AtPIP2;6 increased P_{os} when expressed alone (Fig. 1a, S2). AtPIP1;2, AtPIP1;4 and AtPIP1;5 did not increase P_{os} above control levels when expressed alone, but they further increased P_{os} when co-expressed with AtPIP2;1; with AtPIP1;2 and AtPIP1;5 bing the most effective at increasing P_{os} (Fig. 1b, S2)

AtPIP2;1 elicited currents in *X. laevis* oocytes

A survey of some of the PIP aquaporins from Arabidopsis expressed in *X. laevis* oocytes revealed that AtPIP2;1 was not only a water channel, but also was associated with ionic currents in ND96 bath saline (Fig. 2 and S3; at –100 mV: I_m = –795 nA, SEM=65 nA, n=28 oocytes combined from two frogs; controls at –100 mV: I_m = –355 nA, SEM=33 nA, n=32). AtPIP2;1 gave conductances of 10.3 and 11.4 μS in batches of oocytes from two frogs (Fig. 2c, d), which were significantly higher than the control conductance (3 and 4.6 μS). These conductances are measured as the slope of the linear portion of the current versus voltage curve through the reversal potential (crossing the x-axis). AtPIP1;2 and AtPIP2;2 expressing oocytes in ND96 saline did not display ionic conductances that were significantly different from those of water injected controls (Fig. 2a, b, c). When AtPIP2;1 was co-expressed with AtPIP1;2 the ionic conductance was not significantly different to that of water injected

controls (Fig. 2d and S3); however, water permeability was significantly increased when these two PIPs were co-expressed (Fig. 1b).

Additional experiments over a period of four years involving four different experimenters and two laboratories with different sets of cRNA and re-cloned AtPIP2;1 gave similar results for PIP2;1-induced ion conductance. Comparison of amplitudes of water permeabilities and ionic conductances measured in ND96 as a function of the amount cRNA injected showed saturation of both P_{os} and ionic conductance at higher concentrations of cRNA (Fig. 3a). The data were fitted to the Michaelis-Menten equation and indicated close similarity between the responses of ionic conductance and P_{os} with the amount of cRNA injected. This is reflected in the linear relationship between ionic conductance and P_{os} shown in Fig. 3b.

Given that PIP2;1 induced a much higher water permeability in oocytes compared to water injected controls (Figure 1), we tested the possibility that a slight imbalance in bathing medium osmolality from isotonic may induce a swelling response in the PIP2;1 expressing oocytes that could have activated a native oocyte channel or transporter. For a 50 mosmol kg^{-1} reduction in osmolality (from 234 to 183 mosmol kg^{-1}) neither the controls nor PIP2;1 injected oocytes showed any change in current voltage curve characteristic when bathed in 50 mM NaCl or 50 mM $NaNO_3$ solutions (Fig. S4).

AtPIP2;1 water permeability and conductance were affected by a glycine to tryptophan mutation at residue 103

Previously we showed that a naturally occurring PIP from grapevine (*Vitis vinifera* L. cv Cabernet Sauvignon) was non-functional as a water channel when expressed in *X. laevis* (Shelden et al., 2009*)*. This was due to a tryptophan substituting for a glycine in Loop B,

which was suggested to block the water pore based on a homology model of SoPIP2;1 (Shelden et al., 2009). This mutation (G100W in VvPIP2;1 corresponding to G103W in AtPIP2;1) was previously tested for AtPIP2;1 to explore CO_2 permeation induced by AtPIP2;1 in *X. laevis* oocytes (Wang et al., 2016). We tested the effect of the G103W mutation on water permeation using oocyte swelling assays. The AtPIP2;1 G103W mutant did not induce an increase in water permeability when expressed alone (Fig. 4a,c), but when co-expressed with AtPIP1;2 there was an increase in P_{os}; however, not to the level observed for AtPIP2;1 alone or AtPIP1;2:AtPIP2;1 WT (Fig. 4b,c).

This G103W mutation was also tested for effects on the ionic conduction through AtPIP2;1. Current-voltage curves for water injected controls, AtPIP2;1 and AtPIP2;1 G103W expressing *X. laevis* oocytes in a series of solutions were compared to explore the selectivity of the ionic current (Fig. 5). The Na^+ concentration was held approximately constant while Cl^- concentration was varied using MES as a substitute anion. With this sequence of solutions there was no change in conductance of the water injected controls and no significant change in reversal potential (Fig. 5a). AtPIP2;1-expressing oocytes showed increasing conductance as MES was substituted by Cl^- with the inward current increasing more so than the outward current (Fig. 5b). All the curves intersected the control current-voltage curve at approximately –13 mV as an estimate of the reversal potential after subtraction of control current voltage curves. These results are best explained by the current being predominately carried by Na^+ since there was no substantial shift in reversal potential; however, conductance increased with increasing Cl^- concentration, suggesting potential allosteric modulation. The AtPIP2;1 G103W mutant showed a similar response to controls indicating that it did not induce an ionic conductance.

AtPIP2;1 ion currents in *X. laevis* oocytes were carried by Na^+

We further explored the selectivity of the ionic currents by examining changes in reversal potentials (controls subtracted) with changes in NaCl concentrations. Increasing NaCl concentration while keeping the solution isotonic with sorbitol caused a positive shift in the reversal potential (Fig. 6). Four separate experiments are shown in Fig. 6 from four separate frogs and three different experimenters. In every case the reversal potential shifted positive when NaCl concentration was increased at the higher NaCl concentrations. This indicates that the AtPIP2;1 induced currents were predominately carried by Na^+ in these solutions. The reversal potentials were compared with calculated Nernst potentials for Na^+ and Cl^- taking either literature values for internal oocyte concentrations (Weber, 1999), or those that we measured for our oocytes after incubation in ND96 during expression of AtPIP2;1. For all experiments the measured reversal potentials at 10 mM external NaCl were similar to predicted Nernst potentials for Na^+, while at high NaCl concentrations the reversal potentials were sometimes closer to the Cl^- Nernst potential. The Nernst potential for K^+ was –100 mV, using published values for internal K^+ concentration, and –86 mV for our measured internal K^+ concentrations for all solutions used in Fig. 6.

Exploring the selectivity of the AtPIP2;1-induced currents further, we measured the concentration of K^+, Na^+ and Cl^- in oocytes that were incubated in ND96 for 3 days after either injection with water, un-injected or injected with AtPIP2;1 cRNA (10 ng). The internal Na^+ concentration was significantly elevated in AtPIP2;1-injected oocytes compared to both un-injected and water-injected oocytes (Fig. 7a). There was a reduction in K^+ concentration in AtPIP2;1 injected oocytes when compared with un-injected oocytes but not compared to water injected oocytes (Fig. 7b). There were no significant differences observed in Cl^- concentrations (Fig. 7c). The Na^+/K^+ ratio was significantly lower for AtPIP2;1 injected

oocytes relative to controls due to both the increase in Na^+ and decrease in K^+ concentrations (Fig. 7d). It should be noted that the volume of oocytes used to calculate these concentrations was on average 1.21 mm^3 and the mean volume did not differ between water injected and AtPIP2;1 injected oocytes (Fig. S5).

Given that AtPIP2;1 appeared to induced an increase in Na^+ permeability, we examined the net fluxes of Na^+ after a sudden reduction in external NaCl concentration using the microelectrode ion flux estimation (MIFE) technique. This technique works best at low external concentrations of the measured ions, so measurements of Na^+ efflux were performed after reducing the Na^+ concentration from 96 mM to 5 mM while maintaining a constant osmolality. Initial net Na^+ efflux after reducing the NaCl concentration was significantly larger for AtPIP2;1 expressing oocytes compared to controls (2-way repeated measures ANOVA, $P<0.05$) (Fig. 8a, Fig. S6). There was no significant difference between PIP1;2 + PIP2;1 and controls (Fig. 8b), or PIP1;2 and controls ($P>0.05$) (Fig. 8b) consistent with the TEVC results indicating that co-expression of PIP1;2 with PIP2;1 abolishes the ionic conductance (Figure 2).

AtPIP2;1 was permeable to Na^+ when expressed in *Saccharomyces cerevisea*

Saccharomyces cerevisea was used as an alternative heterologous system to explore whether expression of AtPIP2;1 caused increased accumulation of Na^+ as compared with yeast containing empty vectors. Yeast expressing AtPIP2;1 accumulated more Na^+ than yeast containing empty vectors when incubated for 24 h in growth media containing 0.1 M or 0.5 M NaCl (Fig. 9a). At low external Na^+ concentrations yeast K^+ concentration tended to be lower than empty vector controls (Fig. 9b), consistent with the *Xenopus* oocyte results; however, at 0.5 M external NaCl the K^+ concentrations were significantly elevated in the PIP2;1 expressing cells.

AtPIP2;1 ionic conductance was inhibited by divalent cations and protons

As noted above the AtPIP2;1 conductances we observed were relatively small under the solution conditions initially used and compared to other transporters expressed in Xenopus oocytes, such as High-affinity Potassium (K^+) Transporters (HKTs) (Munns et al., 2012; Byrt et al., 2014). It has previously been shown that AtPIP2;1 water permeation is strongly inhibited by Ca^{2+}, other divalent metals including Cd^{2+} and protons (Verdoucq et al., 2008), and that non-selective cation channels in roots have been found to be inhibited by high Ca^{2+} and low pH (Demidchik and Tester, 2002). With this information in mind we tested the possibility that AtPIP2;1-induced conductances may be inhibited by the standard Ca^{2+} concentration (1.8 mM; free Ca^{2+} = 0.6 mM) in ND96 saline, as used in the experiments described above. We measured ionic conductances of water-injected controls and AtPIP2;1 injected oocytes in Ca^{2+} and Cd^{2+} free conditions, and in conditions with various concentrations of Ca^{2+} or 1 mM Cd^{2+} in a modified ND96 solution (96 mM NaCl, 2 mM KCl, 5 mM HEPES (4-(2-hydroxyethyl)-1-piperazineethanesulfonic acid), pH 7.6 with various EGTA-buffered Ca^{2+} or Cd^{2+} concentrations as indicated).

Ca^{2+} and Cd^{2+} inhibited AtPIP2;1 ionic conductance (Fig. 10, S7, S8). A small reduction in conductance is associated with changing external solutions (Fig. 10a). A significant reduction in conductance was observed with the addition of just 50 μM free Ca^{2+} (Fig. 10b). Further increase in free Ca^{2+} to 0.4 mM gave more substantial inhibition (Fig. 10c). We observed that the inward current was more inhibited by Ca^{2+} than the outward current (Fig. S9). External Cd^{2+} at 1 mM inhibited the conductance similarly to high external free Ca^{2+} concentration (Fig. 10d). Examples of the current versus time traces are shown in Fig. S7. We consistently observed higher conductances (slope of the current versus voltage curve through the reversal potential) for AtPIP2;1 injected oocytes when bathed in the lower Ca^{2+}

concentrations. At close to zero Ca^{2+} concentration the mean conductance was 33.3 +/– 2.1 μS (SEM) while water injected controls under these conditions had conductances of 3.96 +/– 0.46 μS SEM. Conductances of individual oocytes in the initial "zero" Ca^{2+} concentration and then when the bath saline was perfused with the higher concentration of Ca^{2+} or Cd^{2+} are included in Fig. S8. These experiments were used to construct a dose response curve for the AtPIP2;1 induced ionic conductance expressed as values relative to the initial conductance in the near zero external Ca^{2+} concentration (Fig. 11a). Complex responses were obtained and were best fitted by a biphasic dose-response curve where about 50% of the conductance was inhibited by very low external Ca^{2+} (IC_{50} = 5.7 μM free Ca^{2+}) and the remainder inhibited by a higher concentration (IC_{50} = 0.32 mM free Ca^{2+}). It should be noted that inhibition was not complete at higher external Ca^{2+} since even at 0.6 mM free external Ca^{2+} (in ND96) there was still a conductance that was significantly higher than that of the water injected controls as was also evidenced by the experiments reported in Fig. 2, 3 and 5. We also investigated the effect of external pH on the PIP2;1 induced current relative to control water-injected oocytes. The conductance of PIP2;1 expressing oocytes relative to that of the water injected controls in the same solution was inhibited by low pH (Fig. 11b). The fitted dose-response curve shown gives an IC_{50} of pH 6.8.

DISCUSSION

The Arabidopsis plasma membrane aquaporin, PIP2;1, conducted both water and ions when expressed in *X. laevis* oocytes (Fig. 2, 3, 5, 10). There was a close correlation between the water permeability induced by PIP2;1 and the ionic conductance when variable amounts of cRNA were injected (Fig. 3). This ionic conductance was not associated with higher water permeability in of itself because it was specifically associated with the expression of

AtPIP2;1, that is, in similar conditions AtPIP2;2, a protein 93.4% identical to AtPIP2;1, also conducted water but did not induce an ionic conductance. A hypo-osmotic gradient induced by reducing the osmolality of the bathing medium did not alter the ionic currents in PIP2;1 injected oocytes or water injected controls. This result indicates that the ionic currents induced by PIP2;1 expression were not as a consequence of a higher water permeability or a swelling response activating native oocyte channels. Furthermore an AtPIP2;1 mutant with a single amino acid substitution in the pore (G103W) did not induce an ionic current (Fig. 4, 5) but was expressed in the oocyte membrane based on the positive interaction with AtPIP1;2. This indicates that the ionic conductance observed for AtPIP2;1 is unlikely to be an artefact of aquaporin associated expression or swelling in *X. laevis* oocytes and that the AtPIP2;1 protein is unlikely to be interacting with another ion transporter to induce the conductance based on the AtPIP2;1 G103W results.

Co-expression of AtPIP2;1 with AtPIP1;2 increased water permeability relative to AtPIP2;1 expression alone, yet abolished ionic conductance and higher Na^+ efflux when associated with AtPIP2;1 (Fig. 1, 2, 8). This provides further evidence that the ionic conductance and Na^+ flux associated with AtPIP2;1 was not an artefact. Interestingly CO_2 permeability induced by NtAQP1 (a PIP1) also seems to be abolished by interaction with NtPIP2;1 and this has been used as an argument for the homotetrameric structure being critical for CO_2 permeation (Otto et al., 2010). AtPIP2;1 is abundant in all Arabidopsis tissues, and was reported to be present in the homomeric form in roots (Prak et al., 2008; Li et al., 2015), but we lack information about the relative proportions of AtPIP2;1 in homo- and heteromeric forms, and involvement of the subunits in complexes with other proteins such as AtPIP1;2 in different plant tissues and in varying environmental conditions (Yaneff et al., 2014; Yaneff et al., 2015).

Xenopus laevis oocytes expressing AtPIP2;1 consistently displayed greater ionic conductance than controls in the presence of NaCl. In response to an increase in external NaCl we observed a positive shift in reversal potential compatible with Na^+ transport through AtPIP2;1 channels (Fig. 5b, 6). There was no evidence of a negative shift in reversal potential associated with increased external Cl^-, but increased conductance of Na^+ in the presence of Cl^- rather than MES indicates that conductance by AtPIP2;1 might require the presence of Cl^-. We also observed that *X. laevis* oocytes and *Saccaromyces cerevisiae* expressing AtPIP2;1 accumulated more Na^+ than control cells in the presence of relatively high external NaCl (Fig. 7, 9). However, the reversal potentials measured in voltage clamp recordings indicated the current is most likely to be a non-selective cation conductance rather than a strictly Na^+ selective conductance. Our data showed that both K^+ and Na^+ concentrations were altered in oocytes and yeast expressing AtPIP2;1. Further research is needed to examine whether AtPIP2;1 conducts other physiologically important monovalent cations such as K^+, NH_4^+, or anions such as NO_3^- or $H_2CO_3^-$. Of central importance will be determining whether AtPIP2;1 conducts ions and the nature of the ion selectivity *in planta*. There is a precedent for dual water and ion conducting aquaporins functioning as non-selective monovalent cation channels. The human AQP1 is a water channel that functions as a non-selective monovalent cation channel when activated by secondary messengers (Anthony et al., 2000; Yool and Campbell, 2012) and AQP6 has been shown to be a NO_3^- selective channel (Ikeda et al., 2002).

We know from previous studies that AtPIP2;1 water permeability is gated by divalent cations such as Ca^{2+} and Cd^{2+} (Verdoucq et al., 2008), and here we demonstrate that AtPIP2;1 ionic conductance is also inhibited by Ca^{2+} and Cd^{2+} (Fig. 10, 11). These observations are reminiscent of the Ca^{2+} block observed for the *Drosophila* dual ion and water conducting aquaporin Big Brain (BIB) (Yanochko and Yool, 2002; 2004). The

signalling role for Ca^{2+} in regulating BIB conductance is likely to be physiologically important in neuronal cell fate determination (Yanochko and Yool, 2004). In plants, where changes in free Ca^{2+} have important signalling roles particularly in response to stress (Sanders et al., 2002; Choi et al., 2014), the inhibition of AtPIP2;1 ionic conductance by Ca^{2+} may be physiologically important.

The biphasic dose-response curve that we observed for external Ca^{2+} inhibition of the ionic conductance in *Xenopus laevis* oocytes is reminiscent of the biphasic curve observed for water permeation through aquaporins in *Beta vulgaris* where a high affinity (IC_{50} = 5 nM) and a lower affinity component (IC_{50} = 200 μM) of Ca^{2+} inhibition on the cytoplasmic face of the membrane was observed (Alleva et al., 2006). A Cd^{2+} binding site (presumed to bind Ca^{2+} *in vivo*) of SoPIP2;1 is located on the N-terminus that stabilises the closed state of the channel by interaction with loop D and loop B (Törnroth-Horsefield et al., 2006). A second Cd^{2+} binding site (also presumed to mediate Ca^{2+} binding *in vivo*) has been identified on the C-terminus interacting with loop D (Frick et al., 2013). Both of these sites are located on the cytoplasmic side and thought to be important in gating the channel. Although it would be tempting to suggest that the biphasic dose response we observed for ionic conductance here could be linked to these two binding sites, it is difficult to reconcile the sidedness of the extracellular effect in our experiments with the intracellular location of the sites identified in prior work. One possibility is that Ca^{2+} and Cd^{2+} may gain access via the ion conducting pore to interact with potentially intracellular sites.

The prospect that ions could permeate AtPIP2;1 *in planta* brings to mind three key particularly interesting physiological implications. The first is a function for AtPIP2;1 in regulating coupled ion and water flow that could drive rapid shrinking responses as occurs during guard cell closing (MacRobbie, 2006; Grondin et al., 2015) or hypoosmotic turgor regulation (Findlay, 2001). The second is at the root epidermis where AtPIP2;1 is highly

expressed and could be considered as a candidate for facilitating the Na^+ currents associated with nonselective cation channels observed in protoplasts from Arabidopsis root cells – which are blocked by H^+ (pK ~ 6) and Ca^{2+} (IC_{50} ~ 0.1 mM), voltage independent, and weakly selective for monovalent cations (Demidchik and Tester, 2002). These characteristics are remarkably similar to the Ca^{2+} and pH sensitivity we have shown for AtPIP2;1 expressed in *X. laevis* oocytes and investigations of the pharmacological profile of the AtPIP2;1 ionic currents may further test this link. The third implication is that AtPIP2;1 becomes a candidate for having a role in the water and ion co-transport into the xylem that sustains water flow in plants in the absence of water potential differences (Wegner, 2014; Fricke, 2015; Wegner, 2015).

Phosphorylation regulates water permeability through AtPIP2;1 (Prado et al., 2013; Grondin et al., 2015) and protein localisation (Prak et al., 2008). This indicates that we need to explore relationships between the AtPIP2;1 phosphorylation state and the ionic conductance via AtPIP2;1. In a previous study, variation in Na^+ sensitivity of yeast expressing CsPIP2;1 was associated with phosphorylation at Ser273 (Jang et al., 2014); and kinase activity regulated HsAQP1 ion channel activity (Zhang et al., 2007). The phosphorylation of tyrosine Y253 in the carboxyl terminal domain of AQP1 is described as a master switch for regulating the responsiveness of AQP1 ion channels to cyclic nucleotide activators (Campbell et al., 2012; Yool and Campbell, 2012). Testing of whether similar secondary messengers influence dual ion and water aquaporin function in plants and animals may be warranted, as links have been reported between (i) cyclic nucleotide levels in roots and phosphorylation of root proteins including aquaporins (Maurel et al., 1995; Isner et al., 2012), and Na^+ uptake (Maathuis and Sanders, 2001); and (ii) between cyclic nucleotide levels and Ca^{2+} and abscisic signalling (Sanders et al., 2002; Dubovskaya et al., 2011).

We have demonstrated that AtPIP2;1 expression induces an ionic conductance in *Xenopus laevis* oocytes that can be carried at least in part by Na^+ and that this can explain the changes in Na^+ concentration in both oocytes and yeast expression systems. The AtPIP2;1-induced ionic conductance is inhibited by Ca^{2+}, Cd^{2+} and protons. This finding necessitates further research to establish whether AtPIP2;1 is part of a subset of plant aquaporins with dual ion and water conducting roles in plants, that may function to couple ion and water flow across key membranes.

ACKNOWLEDGEMENTS

We thank Wendy Sullivan for expert technical assistance and preparation of oocytes. Funding for this research was supported by the Australian Research Council (ARC) in the form of a DECRA for CB (ARC DE150100837). The ARC Centre of Excellence supported the salaries of JB, SH, JQ, and SR through the ARC Centre of Excellence in Plant Energy Biology (CE140100008). The ARC supported the AY through ARC DP160104641 and MG through ARC FT130100709.

REFERENCES

Alleva, K., Niemietz, C.M., Sutka, M., Maurel, C., Parisi, M., Tyerman, S.D., and Amodeo, G. (2006). Plasma membrane of Beta vulgaris storage root shows high water channel activity regulated by cytoplasmic pH and a dual range of calcium concentrations. *Journal of Experimental Botany* 57**,** 609-621.

Anthony, T.L., Brooks, H.L., Boassa, D., Leonov, S., Yanochko, G.M., Regan, J.W., and Yool, A.J. (2000). Cloned human aquaporin-1 is a cyclic GMP-gated ion channel. *Molecular Pharmacology* 57**,** 576-588.

Bose, J., Xie, Y., Shen, W., and Shabala, S. (2013). Haem oxygenase modifies salinity tolerance in Arabidopsis by controlling K+ retention via regulation of the plasma membrane H+-ATPase and by altering SOS1 transcript levels in roots. *Journal of experimental botany* 64**,** 471-481.

Boursiac, Y., Chen, S., Luu, D.T., Sorieul, M., Van Den Dries, N., and Maurel, C. (2005). Early effects of salinity on water transport in Arabidopsis roots. Molecular and cellular features of aquaporin expression. *Plant Physiology* 139**,** 790-805.

Byrt, C.S., Xu, B., Krishnan, M., Lightfoot, D.J., Athman, A., Jacobs, A.K., Watson-Haigh, N.S., Plett, D., Munns, R., and Tester, M. (2014). The Na+ transporter, TaHKT1; 5-D, limits shoot Na+ accumulation in bread wheat. *The Plant Journal* 80**,** 516-526.

Campbell, E.M., Birdsell, D.N., and Yool, A.J. (2012). The activity of human aquaporin 1 as a cGMP-gated cation channel is regulated by tyrosine phosphorylation in the carboxyl-terminal domain. *Molecular pharmacology* 81**,** 97-105.

Choi, W.-G., Toyota, M., Kim, S.-H., Hilleary, R., and Gilroy, S. (2014). Salt stress-induced Ca2+ waves are associated with rapid, long-distance root-to-shoot signaling in plants. *Proceedings of the National Academy of Sciences* 111**,** 6497-6502.

Demidchik, V., and Tester, M. (2002). Sodium fluxes through nonselective cation channels in the plasma membrane of protoplasts from Arabidopsis roots. *Plant physiology* 128**,** 379-387.

Dubovskaya, L.V., Bakakina, Y.S., Kolesneva, E.V., Sodel, D.L., Mcainsh, M.R., Hetherington, A.M., and Volotovski, I.D. (2011). cGMP-dependent ABA-induced stomatal closure in the ABA-insensitive Arabidopsis mutant abi1-1. *New Phytologist* 191**,** 57-69.

Dynowski, M., Mayer, M., Moran, O., and Ludewig, U. (2008). Molecular determinants of ammonia and urea conductance in plant aquaporin homologs. *FEBS letters* 582**,** 2458-2462.

Findlay, G.P. (2001). Membranes and the electrophysiology of turgor regulation. *Functional Plant Biology* 28**,** 619-636.

Frick, A., Jarva, M., Ekvall, M., Uzdavinys, P., Nyblom, M., and Tornroth-Horsefield, S. (2013). Mercury increases water permeability of a plant aquaporin through a non-cysteine-related mechanism. *Biochemical Journal* 454**,** 491-499.

Fricke, W. (2015). The significance of water co-transport for sustaining transpirational water flow in plants: a quantitative approach. *Journal of experimental botany* 66**,** 731-739.

Gerbeau, P., Amodeo, G., Henzler, T., Santoni, V., Ripoche, P., and Maurel, C. (2002). The water permeability of Arabidopsis plasma membrane is regulated by divalent cations and pH. *The Plant Journal* 30**,** 71-81.

Grondin, A., Rodrigues, O., Verdoucq, L., Merlot, S., Leonhardt, N., and Maurel, C. (2015). Aquaporins Contribute to ABA-Triggered Stomatal Closure through OST1-Mediated Phosphorylation. *Plant Cell* 27**,** 1945-1954.

Holm, L.M., Jahn, T.P., Moller, A.L.B., Schjoerring, J.K., Ferri, D., Klaerke, D.A., and Zeuthen, T. (2005). NH3 and NH4+ permeability in aquaporin-expressing Xenopus oocytes. *Pflugers Archiv-European Journal of Physiology* 450**,** 415-428.

Ikeda, M., Beitz, E., Kozono, D., Guggino, W.B., Agre, P., and Yasui, M. (2002). Characterization of aquaporin-6 as a nitrate channel in mammalian cells requirement of pore-lining residue threonine 63. *Journal of Biological Chemistry* 277**,** 39873-39879.

Isner, J.C., Nühse, T., and Maathuis, F.J. (2012). The cyclic nucleotide cGMP is involved in plant hormone signalling and alters phosphorylation of Arabidopsis thaliana root proteins. *Journal of experimental botany***,** ers045.

Jang, H.-Y., Rhee, J., Carlson, J.E., and Ahn, S.-J. (2014). The Camelina aquaporin CsPIP2; 1 is regulated by phosphorylation at Ser273, but not at Ser277, of the C-terminus and is involved in salt-and drought-stress responses. *Journal of plant physiology* 171**,** 1401-1412.

Jayakannan, M., Babourina, O., and Rengel, Z. (2011). Improved measurements of Na+ fluxes in plants using calixarene-based microelectrodes. *Journal of plant physiology* 168**,** 1045-1051.

Kamiya, T., Tanaka, M., Mitani, N., Ma, J.F., Maeshima, M., and Fujiwara, T. (2009). NIP1; 1, an aquaporin homolog, determines the arsenite sensitivity of Arabidopsis thaliana. *Journal of Biological Chemistry* 284**,** 2114-2120.

Li, G., Boudsocq, M., Hem, S., Vialaret, J., Rossignol, M., Maurel, C., and Santoni, V. (2015). The calcium-dependent protein kinase CPK7 acts on root hydraulic conductivity. *Plant, cell & environment* 38**,** 1312-1320.

Loqué, D., Ludewig, U., Yuan, L., and Von Wirén, N. (2005). Tonoplast intrinsic proteins AtTIP2; 1 and AtTIP2; 3 facilitate NH3 transport into the vacuole. *Plant physiology* 137**,** 671-680.

Ma, J.F., Tamai, K., Yamaji, N., Mitani, N., Konishi, S., Katsuhara, M., Ishiguro, M., Murata, Y., and Yano, M. (2006). A silicon transporter in rice. *Nature* 440**,** 688-691.

Maathuis, F.J., and Sanders, D. (2001). Sodium uptake in Arabidopsis roots is regulated by cyclic nucleotides. *Plant Physiology* 127**,** 1617-1625.

Macrobbie, E.A. (2006). Control of volume and turgor in stomatal guard cells. *The Journal of membrane biology* 210**,** 131-142.

Maurel, C., Kado, R.T., Guern, J., and Chrispeels, M.J. (1995). Phosphorylation Regulates the Water Channel Activity of the Seed-Specific Aquaporin Alpha-Tip. *Embo Journal* 14**,** 3028-3035.

Munns, R., James, R.A., Xu, B., Athman, A., Conn, S.J., Jordans, C., Byrt, C.S., Hare, R.A., Tyerman, S.D., and Tester, M. (2012). Wheat grain yield on saline soils is improved by an ancestral Na+ transporter gene. *Nature biotechnology* 30**,** 360-364.

Nelson, B.K., Cai, X., and Nebenführ, A. (2007). A multicolored set of in vivo organelle markers for co-localization studies in Arabidopsis and other plants. *The Plant Journal* 51**,** 1126-1136.

Newman, I. (2001). Ion transport in roots: measurement of fluxes using ion-selective microelectrodes to characterize transporter function. *Plant, cell & environment* 24**,** 1-14.

Otto, B., Uehlein, N., Sdorra, S., Fischer, M., Ayaz, M., Belastegui-Macadam, X., Heckwolf, M., Lachnit, M., Pede, N., Priem, N., Reinhard, A., Siegfart, S., Urban, M., and Kaldenhoff, R. (2010). Aquaporin Tetramer Composition Modifies the Function of Tobacco Aquaporins. *Journal of Biological Chemistry* 285**,** 31253-31260.

Prado, K., Boursiac, Y., Tournaire-Roux, C., Monneuse, J.M., Postaire, O., Da Ines, O., Schaffner, A.R., Hem, S., Santoni, V., and Maurel, C. (2013). Regulation of Arabidopsis Leaf Hydraulics Involves Light-Dependent Phosphorylation of Aquaporins in Veins. *Plant Cell* 25**,** 1029-1039.

Prak, S., Hem, S., Boudet, J., Viennois, G., Sommerer, N., Rossignol, M., Maurel, C., and Santoni, V. (2008). Multiple phosphorylations in the C-terminal tail of plant plasma membrane aquaporins. *Molecular & Cellular Proteomics* 7**,** 1019-1030.

Preuss, C.P., Huang, C.Y., and Tyerman, S.D. (2011). Proton-coupled high-affinity phosphate transport revealed from heterologous characterization in Xenopus of barley-root plasma membrane transporter, HvPHT1; 1. *Plant, cell & environment* 34**,** 681-689.

Rivers, R.L., Dean, R.M., Chandy, G., Hall, J.E., Roberts, D.M., and Zeidel, M.L. (1997). Functional analysis of nodulin 26, an aquaporin in soybean root nodule symbiosomes. *Journal of Biological Chemistry* 272**,** 16256-16261.

Sanders, D., Pelloux, J., Brownlee, C., and Harper, J.F. (2002). Calcium at the crossroads of signaling. *The Plant Cell* 14**,** S401-S417.

Shabala, S., Shabala, L., Bose, J., Cuin, T., and Newman, I. (2013). Ion flux measurements using the MIFE technique. *Plant Mineral Nutrients: Methods and Protocols***,** 171-183.

Shelden, M.C., Howitt, S.M., Kaiser, B.N., and Tyerman, S.D. (2009). Identification and functional characterisation of aquaporins in the grapevine, Vitis vinifera. *Functional Plant Biology* 36**,** 1065-1078.

Sorieul, M., Santoni, V., Maurel, C., and Luu, D.T. (2011). Mechanisms and Effects of Retention of Over-Expressed Aquaporin AtPIP2; 1 in the Endoplasmic Reticulum. *Traffic* 12**,** 473-482.

Sutka, M., Li, G.W., Boudet, J., Boursiac, Y., Doumas, P., and Maurel, C. (2011). Natural Variation of Root Hydraulics in Arabidopsis Grown in Normal and Salt-Stressed Conditions. *Plant Physiology* 155**,** 1264-1276.

Takano, J., Wada, M., Ludewig, U., Schaaf, G., Von Wirén, N., and Fujiwara, T. (2006). The Arabidopsis major intrinsic protein NIP5; 1 is essential for efficient boron uptake and plant development under boron limitation. *The Plant Cell* 18**,** 1498-1509.

Törnroth-Horsefield, S., Wang, Y., Hedfalk, K., Johanson, U., Karlsson, M., Tajkhorshid, E., Neutze, R., and Kjellbom, P. (2006). Structural mechanism of plant aquaporin gating. *Nature* 439**,** 688-694.

Tournaire-Roux, C., Sutka, M., Javot, H., Gout, E., Gerbeau, P., Luu, D.-T., Bligny, R., and Maurel, C. (2003). Cytosolic pH regulates root water transport during anoxic stress through gating of aquaporins. *Nature* 425**,** 393-397.

Uehlein, N., Lovisolo, C., Siefritz, F., and Kaldenhoff, R. (2003). The tobacco aquaporin NtAQP1 is a membrane CO2 pore with physiological functions. *Nature* 425**,** 734-737.

Verdoucq, L., Grondin, A., and Maurel, C. (2008). Structure–function analysis of plant aquaporin AtPIP2; 1 gating by divalent cations and protons. *Biochemical Journal* 415**,** 409-416.

Verdoucq, L., Rodrigues, O., Martiniere, A., Luu, D.T., and Maurel, C. (2014). Plant aquaporins on the move: reversible phosphorylation, lateral motion and cycling. *Current Opinion in Plant Biology* 22**,** 101-107.

Wang, C., Hu, H., Qin, X., Zeise, B., Xu, D., Rappel, W.-J., Boron, W.F., and Schroeder, J.I. (2016). Reconstitution of CO2 regulation of SLAC1 anion channel and function of CO2-permeable PIP2; 1 aquaporin as carbonic anhydrase 4 interactor. *The Plant Cell***,** TPC2015-00637-RA.

Weaver, C.D., Shomer, N.H., Louis, C.F., and Roberts, D.M. (1994). Nodulin 26, a nodule-specific symbiosome membrane protein from soybean, is an ion channel. *Journal of Biological Chemistry* 269**,** 17858-17862.

Weber, W.-M. (1999). Ion currents of Xenopus laevis oocytes: state of the art. *Biochimica et Biophysica Acta (BBA)-Biomembranes* 1421**,** 213-233.

Wegner, L.H. (2014). Root pressure and beyond: energetically uphill water transport into xylem vessels? *Journal of Experimental Botany* 65**,** 381-393.

Wegner, L.H. (2015). A thermodynamic analysis of the feasibility of water secretion into xylem vessels against a water potential gradient. *Functional Plant Biology* 42**,** 828-835.

Yaneff, A., Sigaut, L., Marquez, M., Alleva, K., Pietrasanta, L.I., and Amodeo, G. (2014). Heteromerization of PIP aquaporins affects their intrinsic permeability. *Proceedings of the National Academy of Sciences of the United States of America* 111**,** 231-236.

Yaneff, A., Vitali, V., and Amodeo, G. (2015). PIP1 aquaporins: Intrinsic water channels or PIP2 aquaporin modulators? *FEBS letters* 589**,** 3508-3515.

Yanochko, G.M., and Yool, A.J. (2002). Regulated Cationic Channel Function in XenopusOocytes Expressing Drosophila Big Brain. *The Journal of neuroscience* 22**,** 2530-2540.

Yanochko, G.M., and Yool, A.J. (2004). Block by extracellular divalent cations of Drosophila big brain channels expressed in Xenopus oocytes. *Biophysical journal* 86**,** 1470-1478.

Yool, A.J., and Campbell, E.M. (2012). Structure, function and translational relevance of aquaporin dual water and ion channels. *Molecular aspects of medicine* 33**,** 553-561.

Zhang, W., Zitron, E., Hömme, M., Kihm, L., Morath, C., Scherer, D., Hegge, S., Thomas, D., Schmitt, C.P., and Zeier, M. (2007). Aquaporin-1 channel function is positively regulated by protein kinase C. *Journal of Biological Chemistry* 282**,** 20933-20940.

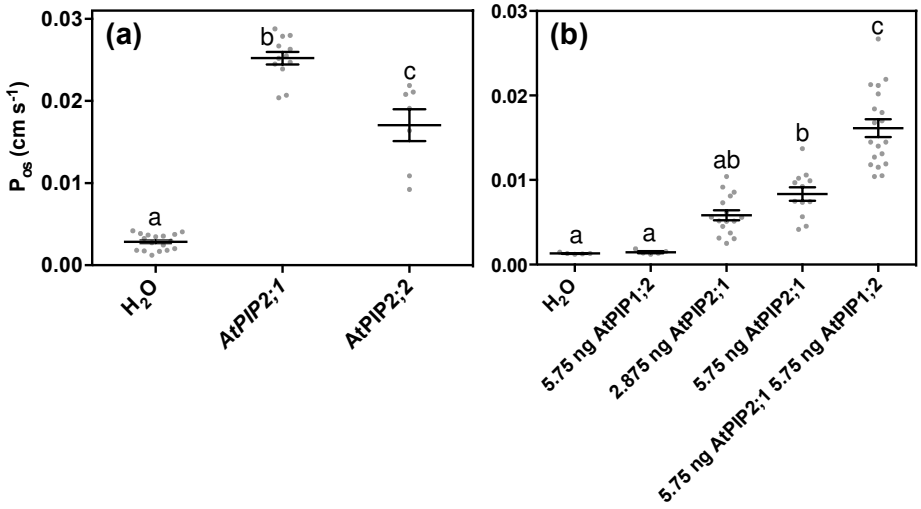

Figure 1. PIP-induced swelling of *X. laevis* oocytes is dependent on PIP-isoform and the amount of cRNA injected. Osmotic water permeabilities (P_{os}) from oocyte swelling experiments comparing AtPIP2;1, AtPIP2;2, AtPIP1;2, and co-expressed AtPIP1;2 and AtPIP2;1, compared to water injected controls. (a) AtPIP2;1 and AtPIP2;2 (11.5 ng cRNA each). (b) AtPIP2;1 and AtPIP1;2, and co-expression with cRNA amounts indicated. Significant differences ($P<0.05$) are indicated by different letters using one way ANOVA with Holm-Sidak's multiple comparisons test. Individual data points and mean +/– SEM, n = 5 to 20 oocytes from two frogs are shown.

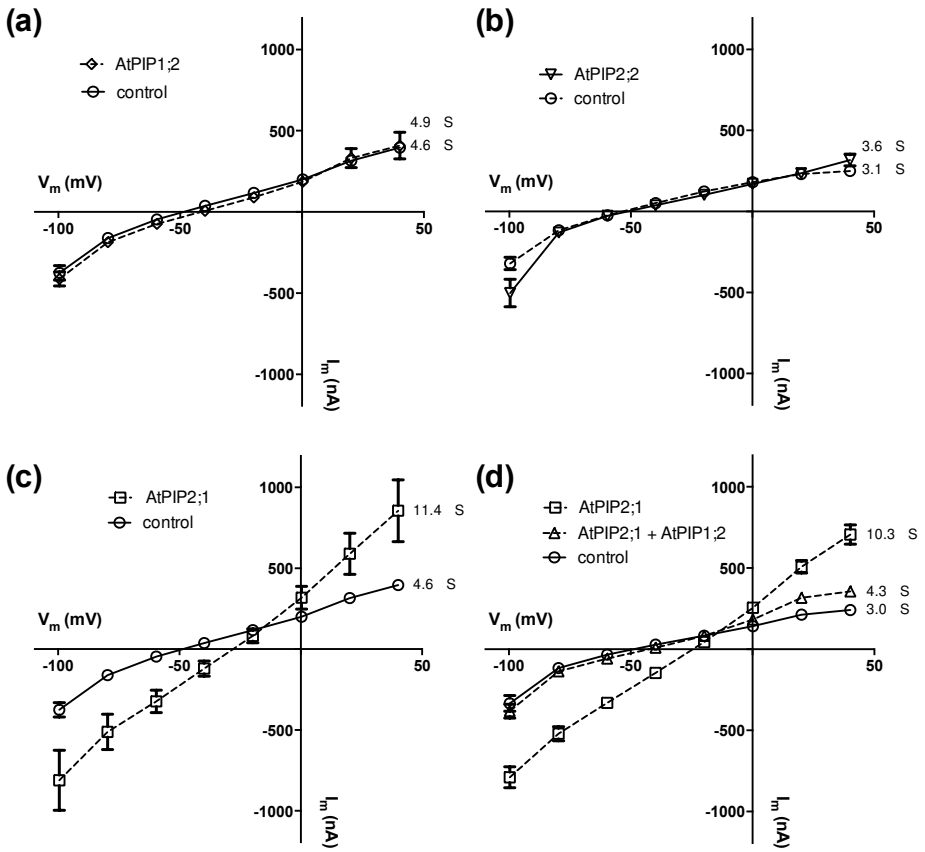

Figure 2. AtPIP2;1 elicits ionic currents when heterologously expressed in *X. laevis* oocytes. Steady state current-voltage curves of *X. laevis* oocytes injected with (a) *AtPIP1;2*, (b) *AtPIP2;2*, (c) *AtPIP2;1* and (d) *AtPIP1;2* and *AtPIP2;1* cRNA in ND96 (pH 7.5). Currents are from oocytes injected with water or cRNA (6 ng per oocyte) from the same batch. Conductances are indicated for the linear part of the curves across the reversal potential. Mean +/– SEM. a) n = 17 for controls, n = 13 for PIP1;2 b) n = 5 for controls, n = 5 for PIP2;2 c) Same controls as (a), n = 7 for PIP2;1 d) n = 15 for controls, n = 21 for PIP2;1 and n = 20 for PIP2;1 coexpressed with PIP1;2. For AtPIP2;1 expressing oocytes, at –100 mV: I_m = –795 nA, SEM=65 nA, n=28 oocytes combined from two frogs; controls at –100 mV: I_m = –355 nA, SEM=33 nA, n=32.

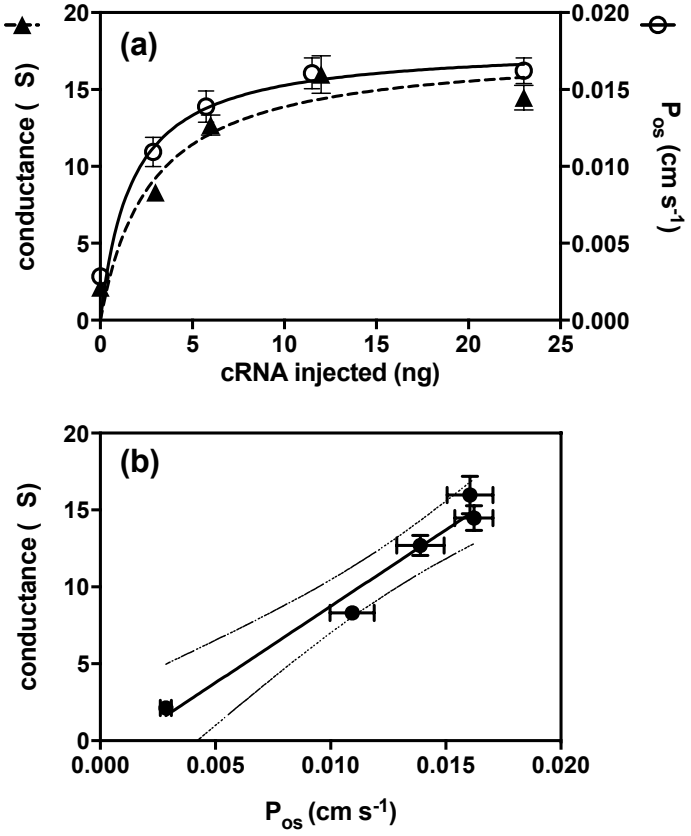

Figure 3. Water and ion transport of oocytes display similar dependence on the amount of AtPIP2;1 cRNA injected. a) Ionic conductance (left y-axis, solid triangles) for *X. laevis* oocytes expressing AtPIP2;1 in ND96 pH 7.5 compared with P_{os} (swelling in 1/5 ND96 pH 7.5) (right y-axis, open circles) as a function of cRNA injected (n =11 – 17 oocytes for swelling assays, n = 6 – 15 oocytes for conductance in same batch of oocytes). The data was fitted with a Michaelis-Menten curve (R^2=0.92 for conductance and R^2= 0.59 for P_{os}) and fitted parameters were: conductance K_m = 2.75 ng, V_{max} = 17.7 μS; P_{os} K_m = 1.71 ng, V_{max} =0.019 cm s^{-1}. b) The linear relationship between ionic conductance and P_{os} taken from the data in (a) (linear regression +/– 95% confidence intervals, R^2 = 0.97). Mean +/– SEM.

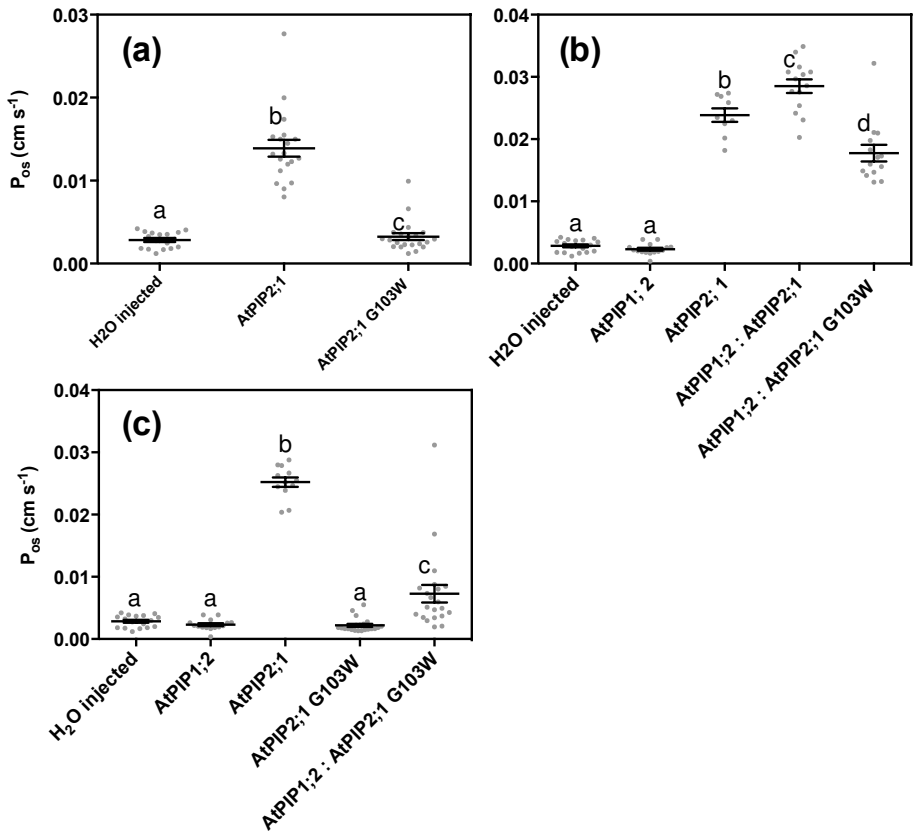

Figure 4. G103W mutation of AtPIP2.1 reduces water permeability. P_{os} comparing AtPIP1;2, AtPIP2;1 and AtPIP2;1 G103W from three separate experiments (frogs). 10 ng of cRNA was injected. a) Comparing AtPIP2;1 with AtPIP2;1 G103W and water injected controls. b) Comparing AtPIP1;2, AtPIP2;1, AtPIP1;2:AtPIP2;1 co-injected, AtPIP1;2:AtPIP2;1 G103W and water injected controls. c) Comparing AtPIP1;2, AtPIP2;1, AtPIP2;1 G103W, AtPIP1;2 : AtPIP21 G103W and water injected controls. Significant differences ($P<0.05$) are indicated by different letters using one way ANOVA with Holm-Sidak's multiple comparisons test. Individual data points and mean +/– SEM are shown.

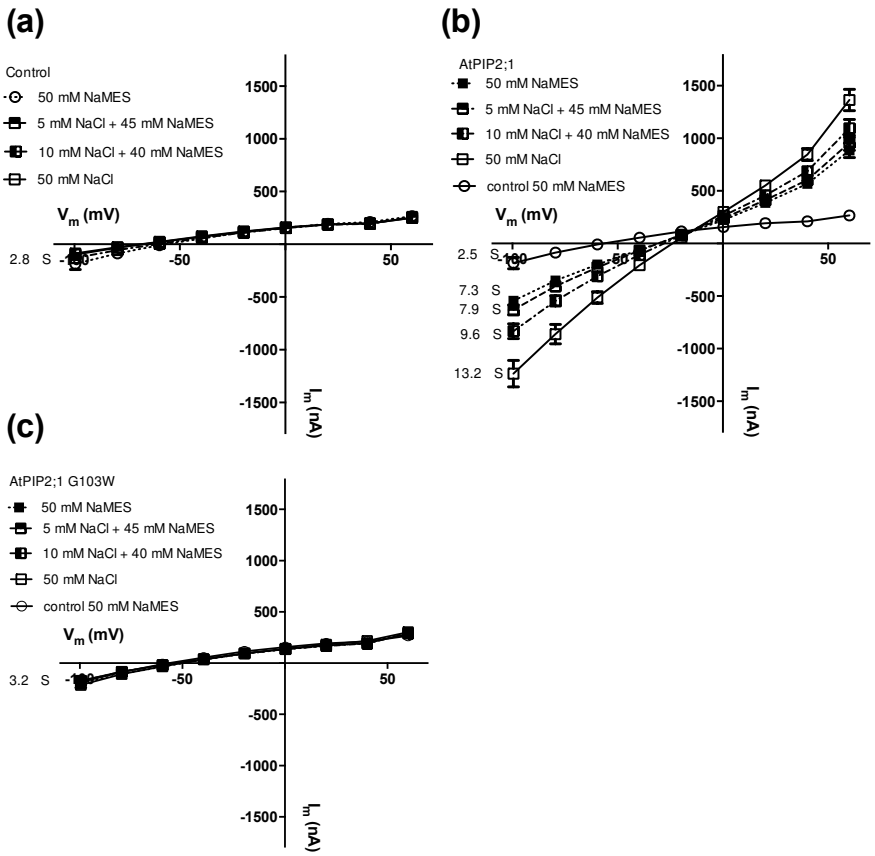

Figure 5. AtPIP2.1 Na^+ conductance is Cl^- dependent, and abolished by G103W substitution. Current-voltage curves (steady state) for (a) water injected controls (n = 4, mean conductance shown for all solutions at the left of the curve), (b) AtPIP2;1 (n = 18) and (c) AtPIP2;1 G103W (n = 10, common conductance shown) in a range of Cl^- concentrations with constant Na^+ concentration, pH 7.5. Conductances shown are for the linear part of curve through the reversal potential. Mean +/– SEM.

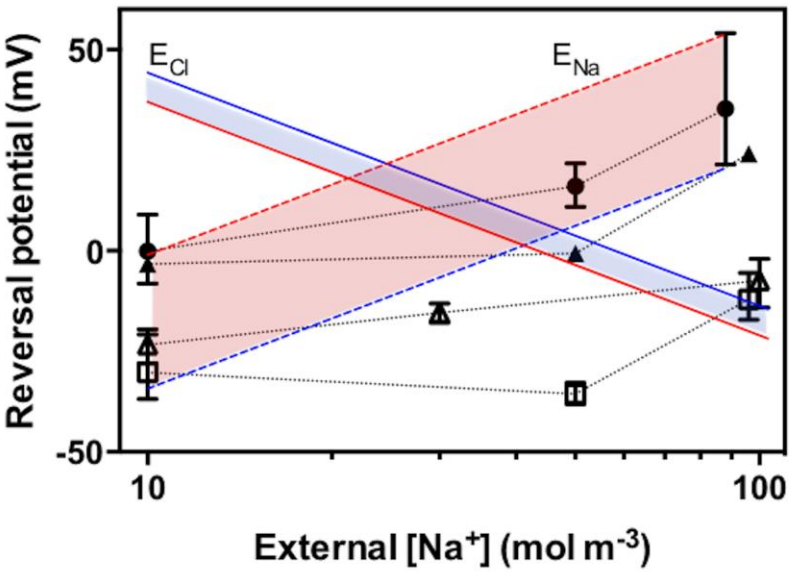

Figure 6. Reversal potentials from a series of two-electrode voltage clamp experiments where the NaCl concentration in the bathing solution was changed. Reversal potentials are plotted against the Na^+ concentration (log scale) since Cl^- concentration was slightly higher from other salts in the buffer. The reversal potentials were taken as the intersection with control current-voltage curves. Same symbols connected by dotted lines indicate the same oocytes (n = 3 to 8 oocytes) from the same frog. Also shown are Nernst potentials for Na^+ (dashed lines, red shade) and Cl^- (solid lines, blue shade) based on literature values for internal oocyte concentrations (red lines) and those calculated from our measurements of internal concentration (blue lines). Error bars, where indicated, are 95% confidence intervals of the reversal potential based on linear regressions through the linear part of the current-voltage curves that cross the voltage axis (controls subtracted).

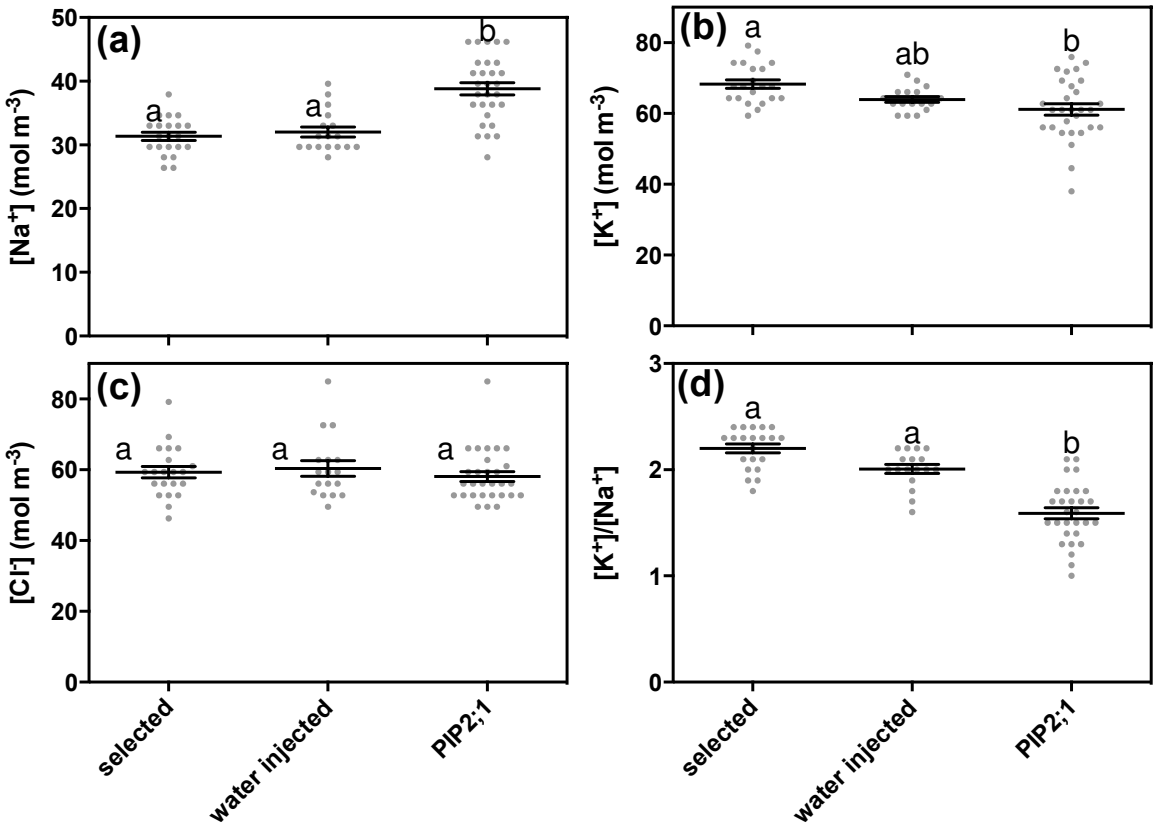

Figure 7. Expression of AtPIP2.1 alters the internal Na^+ concentration of *X. laevis* oocytes. Internal oocyte ion concentrations measured on oocytes after incubation in 96 mM Na^+ for three days for un-injected oocytes, water injected oocytes and AtPIP2;1 cRNA injected (10 ng) oocytes. a) Na^+ concentrations, b) K^+ concentrations, c) Cl^- concentrations, d) Na^+/K^+ ratio. In each case the error bars indicate the range of the data, while the box indicates the SEM of the mean (horizontal internal bar) for n = 21 (un-injected), n = 17 (water injected), n = 29 (cRNA injected). Significant differences were determined by one-way ANOVA, Significant differences ($P<0.05$) are indicated by different letters using one way ANOVA with Holm-Sidak's multiple comparisons test. Individual data points and mean +/– SEM are shown.

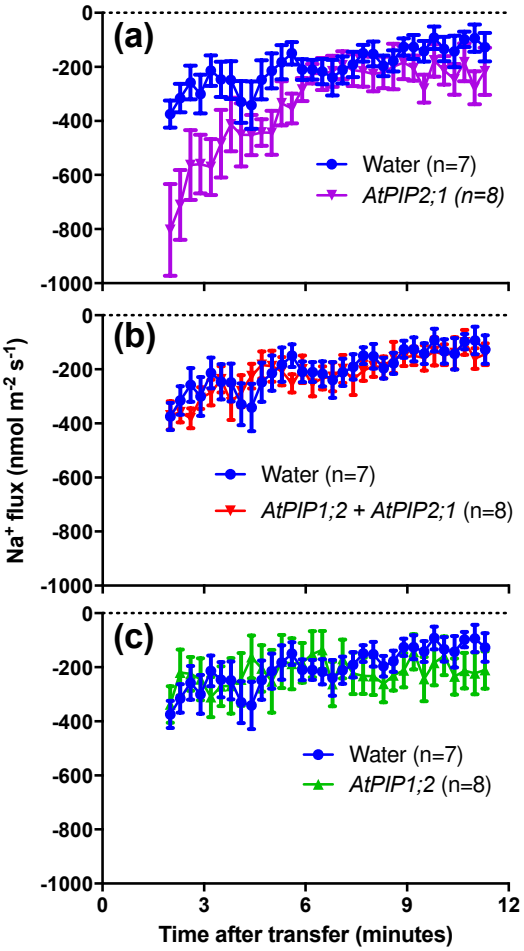

Figure 8. Decreasing external NaCl concentration resulted in a larger Na^+ efflux from AtPIP2;1 expressing oocytes compared to controls. Larger Na^+ efflux was observed for AtPIP2;1 expressing oocytes relative to water injected oocytes (a), AtPIP2;1 + AtPIP1;2 co-injected (b) and AtPIP1;2 injected oocytes (c). Na^+ efflux (indicated as a negative flux) as a function of time after transferring oocytes from ND96 (containing 96 mM NaCl) to a solution consisting of 5 mM NaCl, 2 mM KCl, 50 µM $CaCl_2$, 5 mM HEPES pH 7.5 isotonic which was with ND96 (mannitol, 231 mosmol/kg). In (a), (b) and (c) the water injected control oocytes are the same data, and shown for comparison with gene-injected oocytes. The fluxes were obtained using the microelectrode ion flux estimation (MIFE) technique, electrodes were placed adjacent to the animal pole of the oocyte. Mean +/– SEM, n = 7-8 oocytes.

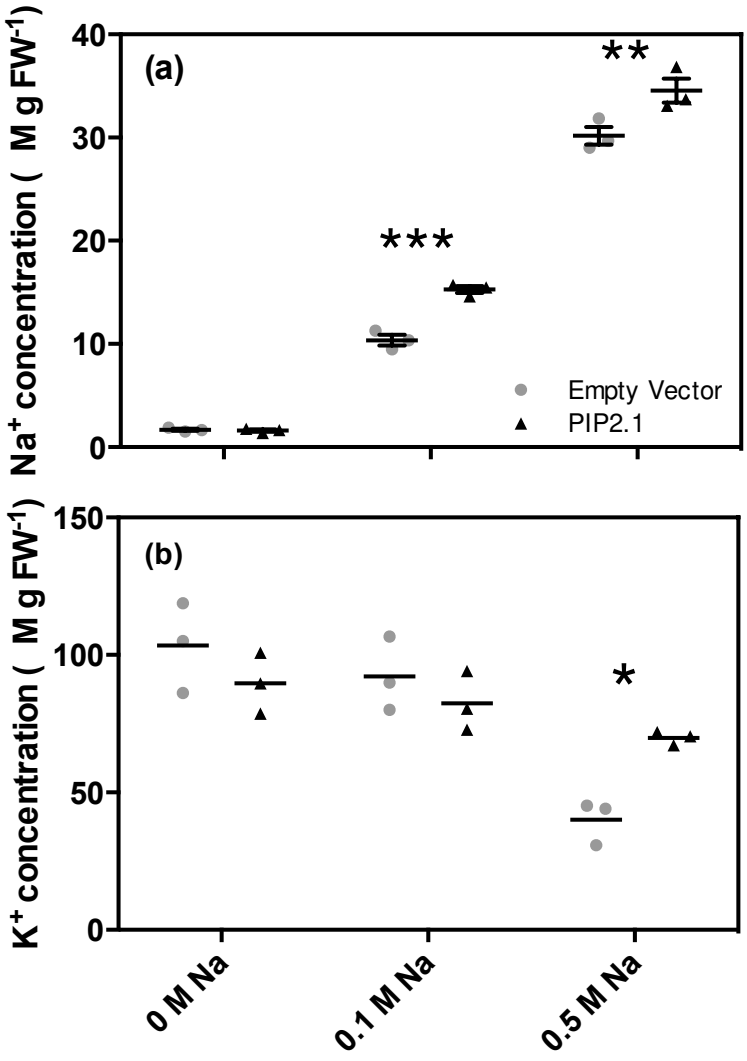

Figure 9. Expression of AtPIP2.1 changes the Na^+/K^+ ratio of yeast cells. Na^+ (a) and K^+ (b) concentrations in yeast empty vector controls or AtPIP2;1 expressing cells at three external Na^+ concentrations. Individual data points and mean +/– SEM are shown. Significant differences between empty vector and PIP2;1 are indicated for each external Na^+ concentration from 2-way ANOVA with Sidak's multiple comparison (* $P<0.05$, ** $P<0.01$, *** $P<0.001$) for 3 replicate batches of cells.

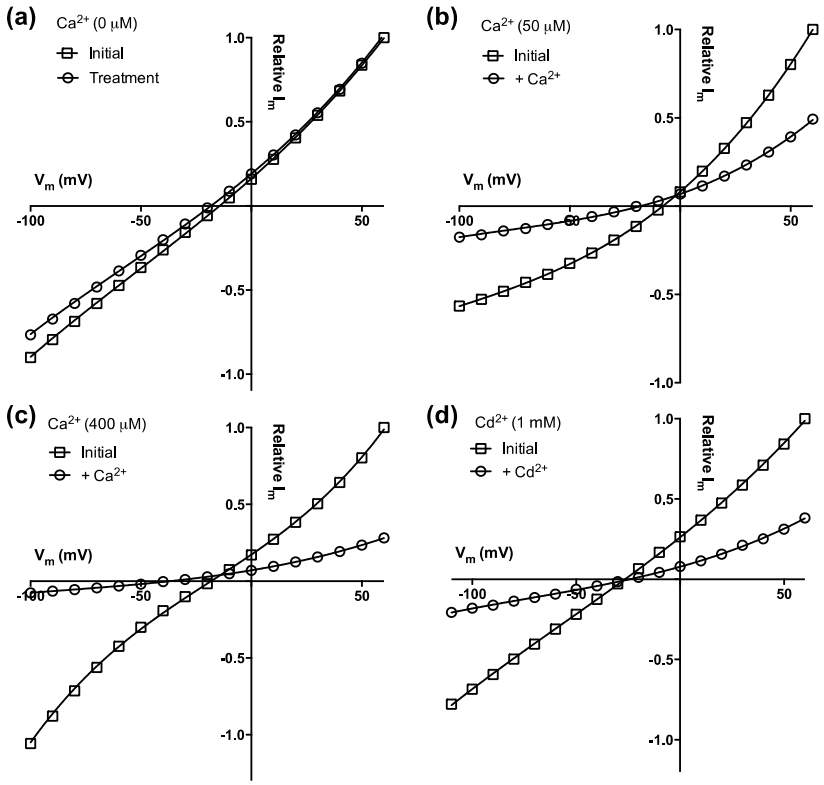

Figure 10. AtPIP2.1 ion currents in *X. laevis* oocytes are inhibited by divalent cations. Examples of current-voltage curves from single oocytes illustrating the effect of external Ca^{2+} and Cd^{2+} on AtPIP2;1 induced currents. In each case the currents are relative (Relative I_m) to the initial current at 60 mV and do not have the water injected control currents subtracted. Zero (effectively) Ca^{2+} and Cd^{2+} concentration is the initial current-voltage curve (square symbol) and the treatment current-voltage curves are after solution replacement with a) 0 μM external Ca^{2+}; b) 50 μM external Ca^{2+}; c) 400 μM external Ca^{2+}; d) 1 mM external Cd^{2+}.

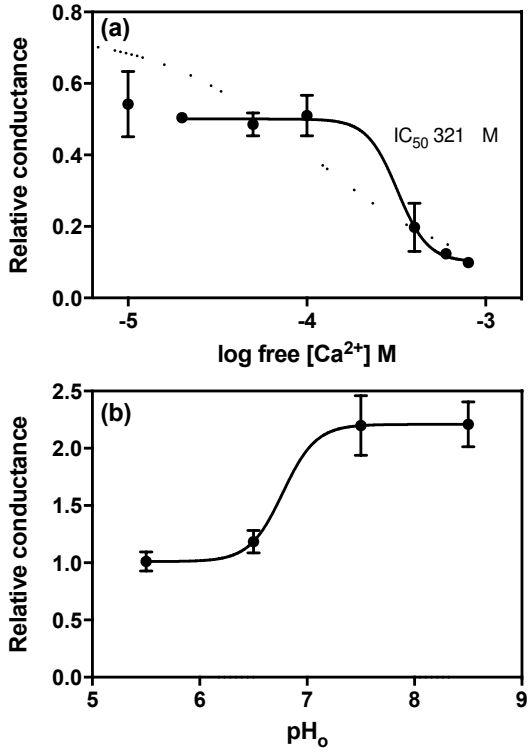

Figure 11. External Ca^{2+} (a) and pH (b) dose-response relationships for the ionic conductance induced by AtPIP2;1 expressed in *X. laevis* oocytes.

a) The data are expressed relative to the initial conductance from experiments such as those shown in Fig. 10 and Fig. S7. The mean relative conductance in the very low external Ca^{2+} concentration is less than 100%, but not significantly so, because sometimes when substituting with the same solution the conductance decreased slightly. The data have been fitted by a single-component dose-response to all the data from very low Ca^{2+} (dotted line), and to the data for higher Ca^{2+} (solid line, R^2=0.75, IC_{50} = 0.321 mM). Mean +/– SEM, n= 3 to 6 oocytes for each point. b) Ionic conductance for AtPIP2;1 expressing oocytes relative to that of controls in solutions of 10 mM NaMES at pH 5.5, 6.5, 7.5 and 8.5. pH adjusted with Tris-base/MES, free Ca^{2+} approx. 0.6 mM ; Mean +/– SEM n = 6. Dose response curve fitted to the data gives IC50 of pH 6.8.